nanomanufacturing

MDPI

Article

Glucose Oxidation Performance of Zinc Nano-Hexagons Decorated on TiO_2 Nanotube Arrays

Ke Wang and Hoda Amani Hamedani *

Department of Materials Science and Engineering, Case Western Reserve University, Cleveland, OH 44106, USA; kxw299@case.edu

* Correspondence: hxa260@case.edu

Abstract: Electrochemically anodized TiO_2 nanotube arrays (NTAs) were used as a support material for the electrodeposition of zinc nanoparticles. The morphology, composition, and crystallinity of the materials were examined using scanning electron microscopy (SEM). Electrochemical impedance spectroscopy (EIS) was performed to evaluate the electrochemical properties of TiO_2 NTAs. Annealing post-anodization was shown to be effective in lowering the impedance of the TiO_2 NTAs (measured at 1 kHz frequency). Zinc nanohexagons (NHexs) with a mean diameter of ~300 nm and thickness of 10–20 nm were decorated on the surface of TiO_2 NTAs (with a pore diameter of ~80 nm and tube length of ~5 µm) via an electrodeposition process using a zinc-containing deep eutectic solvent. EIS and CV tests were performed to evaluate the functionality of zinc-decorated TiO_2 NTAs (Zn/TiO_2 NTAs) for glucose oxidation applications. The Zn/TiO_2 NTA electrocatalysts obtained at 40 °C demonstrated enhanced glucose sensitivity (160.8 µA mM^{-1} cm^{-2} and 4.38 µA mM^{-1} cm^{-2}) over zinc-based electrocatalysts reported previously. The Zn/TiO_2 NTA electrocatalysts developed in this work could be considered as a promising biocompatible electrocatalyst material for in vivo glucose oxidation applications.

Keywords: titania nanotube arrays; zinc nanoparticles; electrodeposition; glucose oxidation

Citation: Wang, K.; Amani Hamedani, H. Glucose Oxidation Performance of Zinc Nano-Hexagons Decorated on TiO_2 Nanotube Arrays. *Nanomanufacturing* **2024**, *4*, 187–201. https://doi.org/10.3390/nanomanufacturing4040013

Academic Editor: Candido Fabrizio Pirri

Received: 1 August 2024
Revised: 28 August 2024
Accepted: 11 September 2024
Published: 4 October 2024

1. Introduction

Diabetes management relies heavily on blood glucose monitoring [1]. Electrochemical glucose sensors are most commonly used today for glucose monitoring due to their high sensitivity, reproducibility, easy maintenance, and low cost [2,3]. Among the most common commercially available glucose sensors, amperometric types have been extensively studied over the past few decades [3,4]. Such sensors are classified as invasive and non-invasive, where the invasive sensors typically work with analytes with higher glucose concentrations (i.e., blood), while the non-invasive sensors deal with analytes with lower glucose concentrations (i.e., sweat) [3]. By measuring the current generated when electrons are exchanged between an electrode and a biological system, amperometric sensors can detect both direct and indirect electron transfers [2,3]. However, both invasive and non-invasive point-of-care measurements are prone to neglecting abrupt spikes in blood glucose concentrations between measurements because they are intermittent measurements. Alternatively, a continuous profile of blood glucose levels can provide a full picture of the patient's condition throughout the day [5]. Therefore, an implantable direct glucose sensing device is required for continuous and accurate glucose monitoring.

Furthermore, an implantable sensor increases the accuracy and clinical relevance of the data as it detects glucose in the intravenous blood rather than in the peripheral blood [2]. Most high-sensitivity glucose sensing materials that have been developed are not biocompatible, thus making it necessary to develop high-performance "biocompatible" glucose sensing materials [6].

Recently, non-enzymatic electrochemical approaches have shown promise in remedying the shortcomings of enzymatic systems for in vivo applications, such as relatively high cost and short lifetime due to the thermal and chemical instability of enzymes [7–11]. For non-enzymatic glucose sensors, using materials like transition metals provides comparable electrochemical sensing properties as the enzymatic systems while maintaining a low cost and higher stability in operation. A number of novel materials have been developed for direct glucose detection in the blood and body fluids. Among various metal-based materials and their oxides, only a limited number (e.g., Ti, Zn, and Ir) have been identified as biocompatible for direct blood contact.

Transition metal oxides have shown to be promising electrode materials in electrochemical applications such as non-enzymatic glucose sensors [12]. On the other hand, these metal oxides also present the challenge of low electrical conductivity and poor ion transport kinetics [13]. Past studies indicate that nanostructures could improve the electrochemical processes due to enhanced charge transfer kinetics. One-dimensional (1D) nanostructures such as nanotubes have recently become popular as electrode architectures for electrochemical devices due to their enhanced nano-scale properties. Materials with 1D nanoporous structures could create a more efficient path for current transfer and facilitate ion diffusion. Furthermore, 1D porous nanostructures could increase the surface area of the electrode material, resulting in a more efficient electrode with a smaller form factor enabling device miniaturization [4,14,15]. An ideal support material should have the following characteristics: (1) high surface area and abundant active sites for catalyst loading, (2) defined pathways for electron transfer, and (3) low cost and facile preparation [16]. Using 1D nanoporous substrates of metals and metal oxides as a vehicle for catalytic reactions via loading catalyst materials (such as metal nanoparticles) appears to meet these characteristics and be a viable option for improving the electrochemical performance of metal oxide-based sensing devices [14–17].

Traditional noble metal electrodes with a smooth surface in glucose oxidizing electrodes are highly biocompatible, but face several challenges such as high cost and inefficient oxidation of glucose [4,18]. Nanomaterials that facilitate the charge transfer process could potentially resolve the sensitivity issues faced by these traditional electrodes [19]. Titania nanotubes are becoming increasingly attractive to electrochemical applications as a supporting material because of their high biocompatibility, wear resistance in an electrochemical environment, and easy fabrication/scalability. Being a transition metal oxide nanostructure, titania nanotube arrays provide a highly ordered nanoporous morphology for the diffusion of charged species [20–23].

While there is a wide selection of metal nanoparticle candidates for use as a catalyst material in glucose oxidation, a limited number of these materials are biocompatible. Among highly sensitive multicomponent non-enzymatic glucose sensing materials, copper-based electrodes (e.g., CuO/Cu, Au/CuO, and Cu_2O/TiO_2 nanotubes) have been reported with high glucose sensitivities: 708.7, 3490.7, and 157.45 $\mu A\ mM^{-1}\ cm^{-2}$, respectively [24–26]. However, copper is not known to be a biocompatible material, and copper oxide has toxicity towards mammalian cells; therefore, it is not ideal for in vivo applications [27].

Zinc compounds have been widely used in optoelectronics and sensor devices [28,29]. Zinc presents a viable biocompatible catalyst material for the electrodes of implantable glucose sensors due to its nontoxicity, chemical stability, and electrochemical activity [28]. Currently, non-enzymatic electrochemical sensing materials require improved electrode performance while maintaining biocompatibility. We have previously reported on the fabrication of biocompatible Zn/TiO_2 NTAs [30]. This work aims to examine the electrocatalytic properties of the previously developed Zn/TiO_2 NTAs for the application of glucose oxidation. Biocompatible metal nanoparticles, such as zinc, decorated on biocompatible titania nanotube arrays could constitute a multifunctional electrode material system for potential applications in non-enzymatic implantable glucose biosensors.

2. Experimental Methods

2.1. Titania Nanotube Arrays Fabrication

TiO_2 nanotube arrays (hereafter referred to as TiO_2 NTAs) were fabricated using an electrochemical anodization process. The anodization was performed at 40 V in a two-electrode setup with polished titanium foils (>99.98%, Sigma-Aldrich, St. Louis, MO, USA) as the anode and a platinum foil (99.99%, BTC, Hudson, NH, USA) as the cathode in the electrolyte solution, with 0.5 wt% of ammonium fluoride (NH_4F), 3 vol% of D.I. water, and 96 vol% of ethylene glycol. The anodization process was carried out in two steps. The first anodization was conducted at 40 V for 1 h. Then, the nanotubes were removed by ultrasonication in D.I. water to generate footprints on the titanium substrate. The second anodization was carried out at 40 V for 30 min to produce a high-quality nanotube layer. A group of two-step as-anodized TiO_2 NTA samples were then annealed at 450 °C for 4 h in air using a Lindberg/Blue MTM Mini-Mite Tube Furnace to convert the amorphous TiO_2 nanotubes to crystalline anatase. The one-step as-anodized TiO_2 NTA samples were named "one-step anodized/as-anodized" or briefly "as-anodized", and the two-step as-anodized TiO_2 NTA samples that underwent annealing were named "annealed".

2.2. Electrodeposition of Zinc on TiO_2 NTAs

The zinc electrodeposition process was performed using chronoamperometry in EC-Lab software accompanied with a potentiostat (BioLogic SP-50e, Seyssinet-Pariset, France) at a constant potential of −1.6 V at 40 °C for 5 min in a 3-electrode setup with a TiO_2 NTAs as the working electrode, an Ag/AgCl (Basi. Inc., West Lafayette, IN, USA) electrode as the reference electrode, and a platinum electrode (Basi. Inc., West Lafayette, IN, USA) as the counter electrode. A zinc-containing deep eutectic solvent was used as the electrolyte. $ZnCl_2$ salt was dissolved in an ethaline eutectic mixture (choline chloride and ethylene glycol, 1:2 molar ratio). After the electrodeposition, the deposited sample was taken out and rinsed with isopropyl alcohol (IPA) and D.I. water to eliminate the remaining ethaline and possible chlorine on the sample due to surface tension and absorption.

2.3. Microstructure and Compositional Characterization

Morphology and compositional characterization of TiO_2 NTAs and Zn/TiO_2 NTAs was performed using SEM and XRD analyses. Scanning electron microscopy (SEM) analyses were performed using an Apreo2 scanning electron microscope (Thermo Fisher Scientific, Waltham, MA, USA). X-ray diffraction (XRD) was performed to identify the crystalline phases in the samples.

2.4. Electrochemical Measurements

Cyclic voltammetry (CV) tests were carried out using EC-Lab (v11.43) software accompanied with a potentiostat (BioLogic SP-50e) on annealed TiO_2 NTAs and 40 °C-deposited Zn/TiO_2 NTA samples in 0.1 M NaOH with different glucose concentrations, since non-enzymatic glucose sensing materials perform favorably in alkaline environments [31]. In addition, an NaOH concentration of 0.1 M has been reported to be optimal for glucose oxidation in an alkaline medium [32]. The Zn/TiO_2 NTA sample served as the working electrode. An Ag/AgCl (Basi. Inc., West Lafayette, IN, USA) electrode was used as the reference electrode, and a platinum electrode (Basi. Inc., West Lafayette, IN, USA) as the counter electrode. A complete CV scan cycle was established from the 1 V to −0.5 V potential range to reveal redox peaks. A number of CV tests were performed using different scan rates (10 mV s^{-1}–100 mV s^{-1}) to further investigate the redox process at the working electrode surface.

In order to investigate the glucose sensing performance of the samples, chronoamperometry was performed using EC-Lab (v11.43) software accompanied with a potentiostat (BioLogic SP-50e) on TiO_2 NTAs and 40 °C-deposited Zn/TiO_2 NTAs in a 0.1 M NaOH solution with different glucose concentrations at the potential step of 0.7 V, which was determined by experimenting with multiple potentials to obtain a set of chronoamperometry data that presents a sufficient range of linear behavior as well as low noise [31]. After each step of chronoamperometry (100 s), 0.5 mM of glucose (0–5 mM in total) was added to the 0.1 M NaOH solution and stirred with a magnetic stirrer until completely dissolved. With each successive addition of glucose, the change in current response was recorded to determine the glucose sensitivity.

EIS measurements were conducted using EC-Lab (v11.43) software accompanied with a potentiostat (BioLogic SP-50e) on the TiO_2 NTAs and Zn/TiO_2 NTAs. The measurements were carried out in 1X phosphate buffered saline (1X PBS) with the addition of 5 mM glucose to the solution in order to examine the impedance of the samples during glucose oxidation in the simulated physiological environment. Impedance measurements were taken at the 1 kHz frequency to more closely simulate actual in vivo conditions when the material interacts with blood [33]. An AC current of 0.05 A was applied to the working electrode (i.e., TiO_2 NTAs and Zn/TiO_2 NTAs) in the frequency range of 10 kHz–1 Hz, with 25 steps per decade for frequencies higher than 5 Hz, and 7 steps per decade for frequencies lower than 5 Hz.

3. Results

3.1. SEM Results

Figure 1a shows the morphology of the TiO_2 NTAs fabricated using two-step anodization. Part of the two-step as-anodized TiO_2 NTAs was delaminated from the titanium substrate for SEM imaging. The tubes' side walls can be observed in the inset. The average pore size of the TiO_2 NTAs is ~80 nm and the average tube length is ~5 µm. Figure 1b,c shows SEM images of Zn/TiO_2 NTAs (annealed) deposited at room temperature and at 40 °C. The zinc nanoparticles present a hexagonal structure (named hereafter as zinc NHexs) with a thickness of about 10–20 nm and a diameter ranging from about 200 to 400 nm, exhibiting a high aspect ratio with an observable stacked hexagonal platelet morphology.

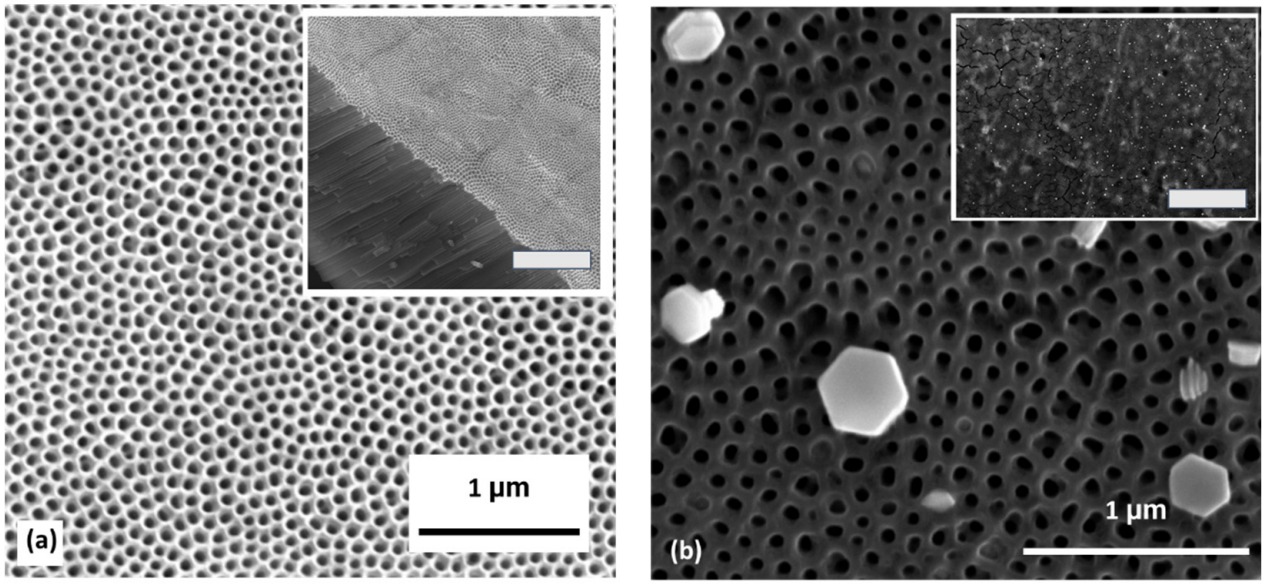

Figure 1. *Cont.*

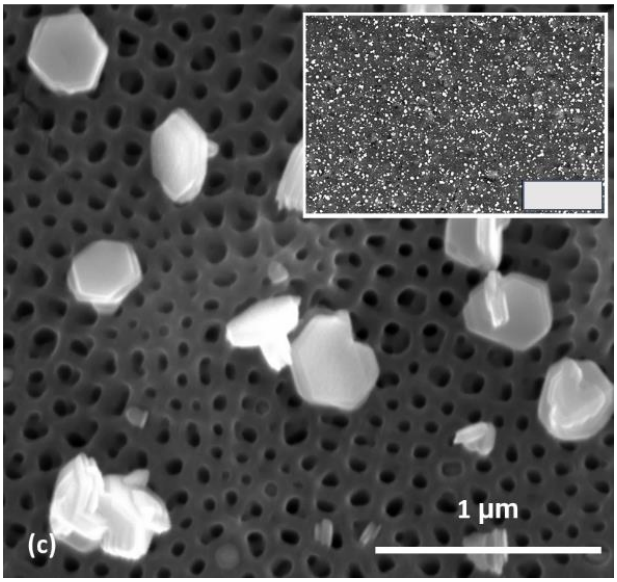

Figure 1. Top-view SEM images of (**a**) annealed TiO_2 NTAs with the inset showing the cross section, (**b**) Zn/TiO_2 NTAs (annealed) deposited at room temperature, and (**c**) Zn/TiO_2 NTAs (annealed) deposited at 40 °C. The scale bars in the insets show (**a**) 2 µm, (**b**) 10 µm, and (**c**) 10 µm, respectively.

3.2. XRD Results

The XRD patterns of TiO_2 NTAs and 40 °C-deposited Zn/TiO_2 NTAs are shown in Figure 2, with peak positions of TiO_2 anatase, zinc, and titanium marked. Crystalline zinc was observed on the Zn/TiO_2 NTAs. The deposition time for the Zn/TiO_2 NTAs used for the XRD was increased to 40 min in order to achieve a thick layer of zinc NHexs.

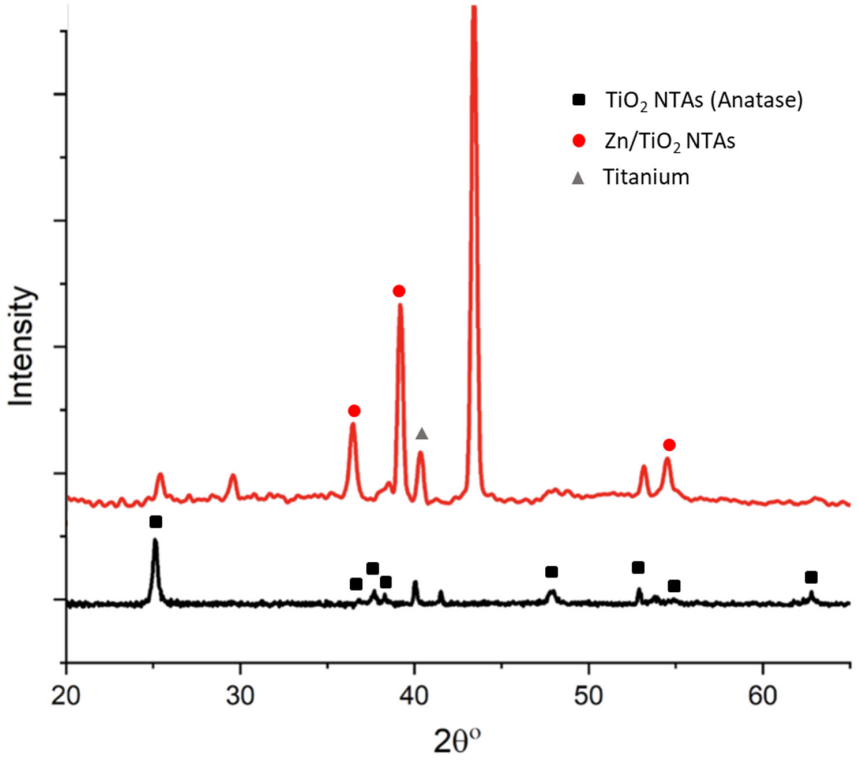

Figure 2. XRD patterns of 40 °C-deposited Zn/TiO_2 NTAs (annealed) reconstructed from our previous work [30], showing zinc peaks with peak positions (circles). The peak positions for TiO_2 (anatase) (squares) and for the titanium (triangle) are identified.

3.3. CV Results

Figure 3 shows that in the CV results with different scan rates of 10–100 mV s^{-1} performed on Zn/TiO_2 NTAs (annealed) in a 0.1 M NaOH solution with 5 mM of glucose, the oxidation current peaks linearly increase with the square root of the scan rates. The starting point and directions for the scans have been marked on the CV plots.

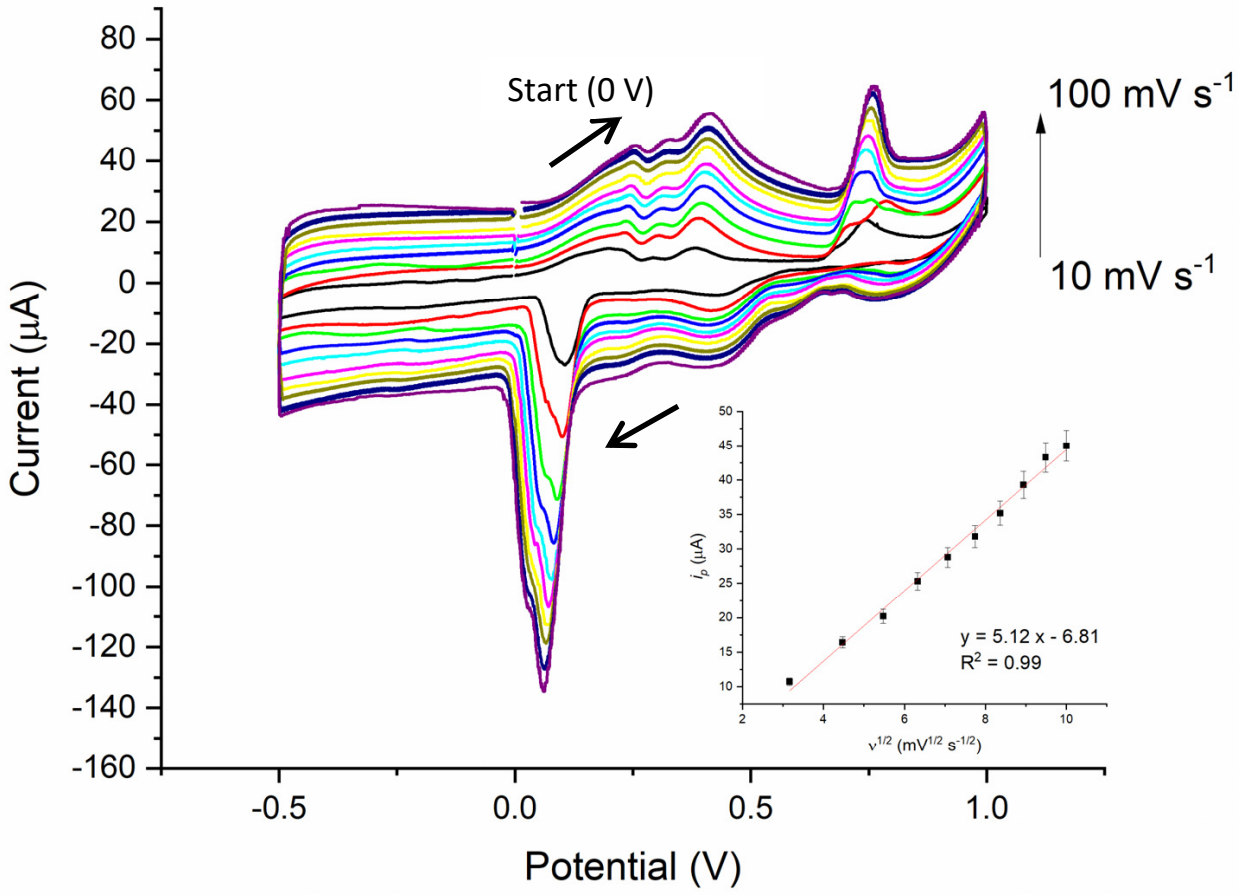

Figure 3. CV of Zn/TiO_2 NTAs in a 0.1 M NaOH solution with 5 mM of glucose in scan rates from 10 mV s^{-1} to 100 mV s^{-1}. Different colors are used to differentiate varying scan rates. The inset is the current peak vs. square root of scan rate, and the red dash line is for an eye guide only.

To investigate the electrochemical reactions occurring at the sample surface, Figure 4 shows the CV curves of bare TiO_2 NTAs and Zn/TiO_2 NTA electrodes in the presence and absence of glucose. The inset CV curve is enlarged, with a limited potential range presented to better present the redox peaks. As shown, the Zn/TiO_2 NTAs present an increased current response in a 0.1 M NaOH solution containing 0 mM and 5 mM of glucose compared to bare TiO_2 NTAs, and the glucose oxidation peak on bare TiO_2 NTAs in a 5 mM glucose environment is observed at 0.24 V (Peak I). From CV plots in Figures 4 and 5, oxidation peaks appear at potentials 0.24 V (Peak I), 0.36 V (Peak II), and 0.68 V (Peak III), and a reduction peak was obtained at 0.02 V (Peak IV). A calibration curve is obtained at 0.24 V in the inset.

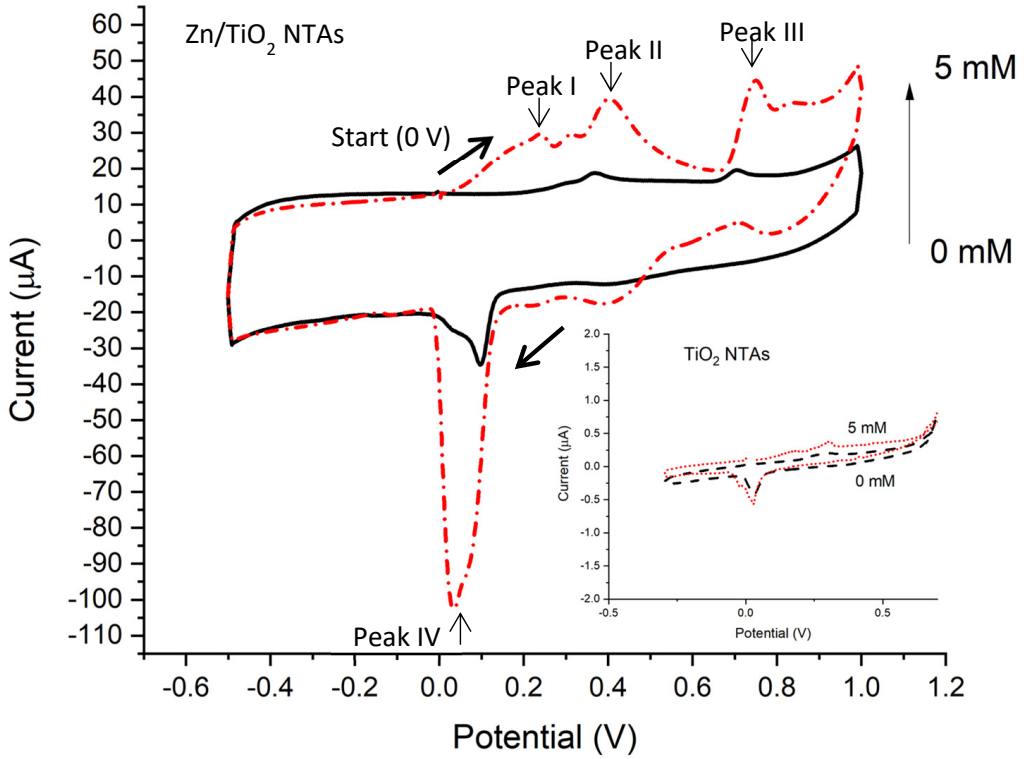

Figure 4. CV of TiO_2 NTAs (inset) and Zn/TiO_2 NTAs in a 0.1 M NaOH solution containing 0 mM and 5 mM of glucose (at a scan rate of 50 mV s^{-1}). The red dashed curve refers to 5 mM glucose concentration, and the black solid curve refers to 0 mM glucose concentration. The arrows indicate potential sweep directions.

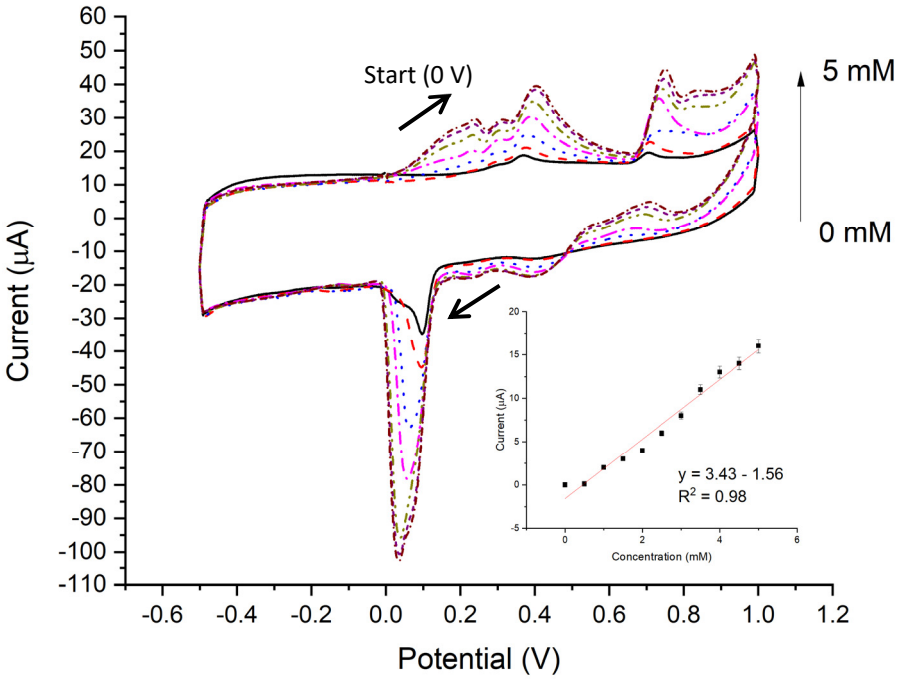

Figure 5. CV on Zn/TiO_2 NTAs in a 0.1 M NaOH solution with different glucose concentrations (at a scan rate of 50 mV s^{-1}). Different colors of the curves refer to the varying glucose concentrations. The inset shows the calibration curve of the oxidation peak's current values. The legends describe glucose concentrations in the 0.1 M NaOH solution.

3.4. EIS Results

Figure 6 shows the normalized impedance plots for NTA samples in a pure 1X PBS solution with 5 mM glucose. The phase angle of the bode plots in Figure 7 approaches the 0 degree near 1 kHz for the annealed samples, exhibiting resistive behavior, while a more capacitive behavior is found near 1 Hz ("0" on the log frequency axis) closer to a 90 degree phase angle.

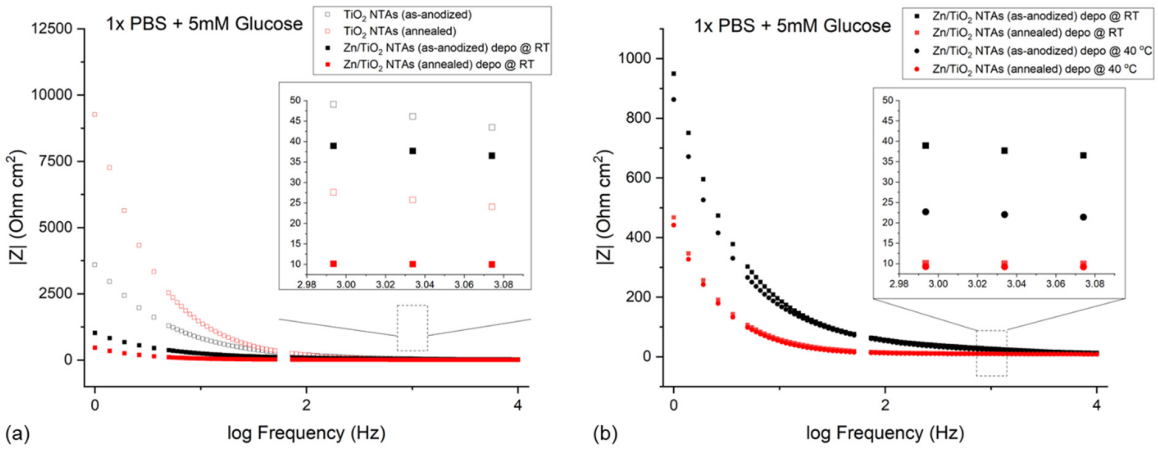

Figure 6. (**a**) Normalized impedance spectra of Zn/TiO_2 NTA samples tested in a pure 1X PBS solution with 5 mM glucose compared to reference TiO_2 NTAs. (**b**) Normalized impedance spectra of Zn/TiO_2 NTA samples deposited under different temperatures tested in a pure 1X PBS solution with 5 mM glucose.

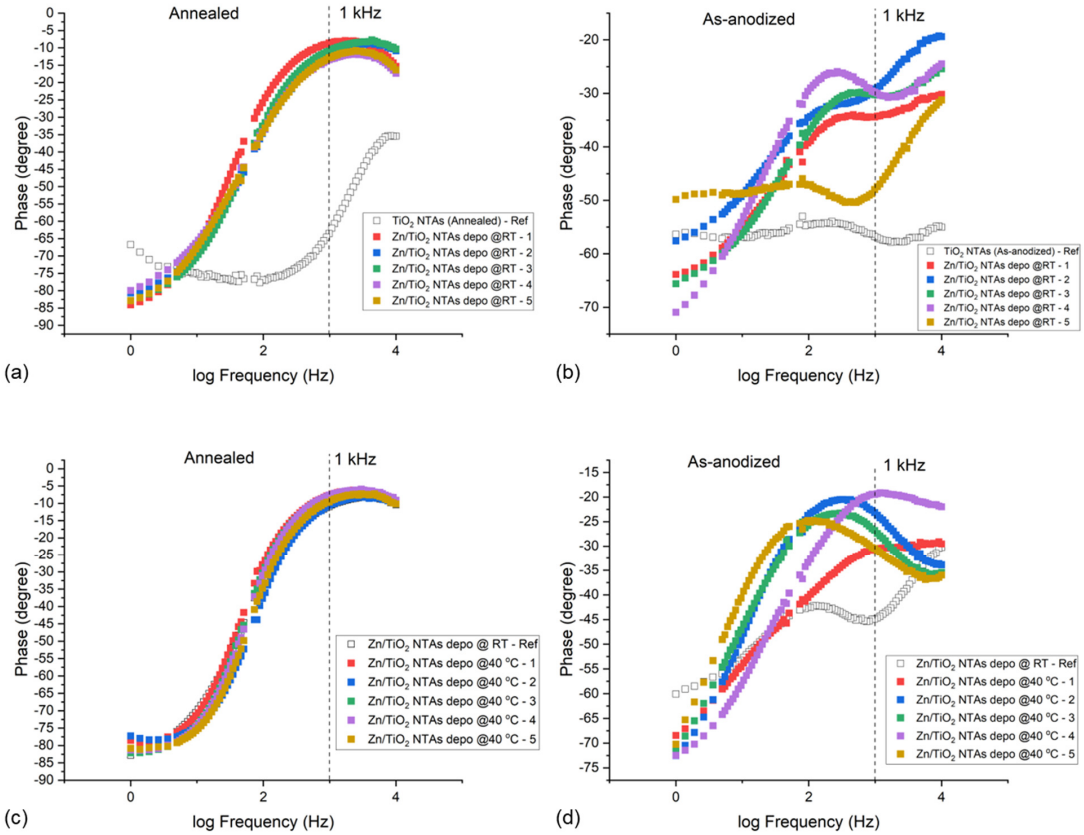

Figure 7. Phase plots for (**a**) Zn/TiO_2 NTAs (annealed), (**b**) Zn/TiO_2 NTAs (as-anodized) with zinc deposited at room temperature, (**c**) Zn/TiO_2 NTAs (annealed), and (**d**) Zn/TiO_2 NTAs (as-anodized) with zinc deposited at 40 °C. EIS was performed in a pure 1X PBS solution + 5 mM glucose.

3.5. Chronoamperometry Results

Figure 8 demonstrates that with the increasing addition of glucose in the 0.1 M NaOH solution, Zn/TiO_2 NTAs have an increasing amperometric response for glucose oxidation when applied with a positive potential (0.7 V). The glucose sensitivity of the Zn/TiO_2 NTAs can be obtained by dividing the slope of the calibration curve of the current–time transient from chronoamperometry tests by the sample area (insets of Figure 8). From a 40 °C-deposited Zn/TiO_2 NTA sample, the glucose sensitivity was calculated to be 160.8 μA mM^{-1} cm^{-2} from the left inset (current value taken at 0.2 s after addition of glucose), and 4.38 μA mM^{-1} cm^{-2} from the right inset (current value taken at 50 s after addition of glucose).

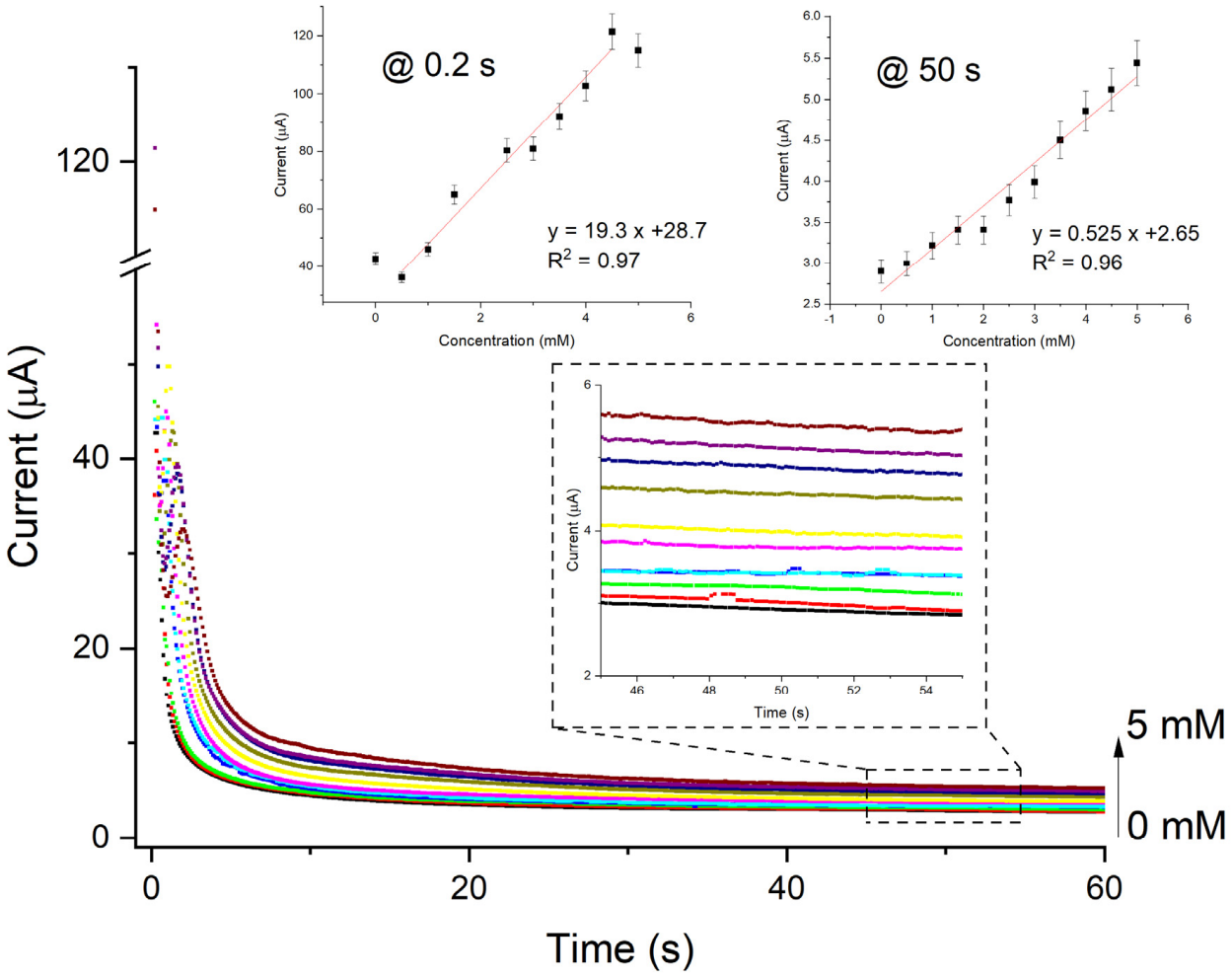

Figure 8. Current–time transient for Zn/TiO_2 NTAs with successive addition of 0.5 mM glucose in a 0.1 M NaOH solution; curves in different colors to differentiate between varying glucose concentrations. The left inset is the calibration curve taken at 0.2 s of each step, and the right inset is the calibration curve taken at 50 s of each step (enlarged in the middle inset). The glucose sensitivity is 160.8 μA mM^{-1} cm^{-2} in the case of the 0.2 s data point and 4.38 μA mM^{-1} cm^{-2} in the case of the 50 s data point.

4. Discussion

4.1. Microstructure and Compositional Characterization

As shown in Figure 1a, a highly ordered nanotube array was achieved. The inset of Figure 1b,c shows that the TiO_2 NTAs underwent a significant increase in the deposition of zinc NHexs at 40 °C compared to room temperature deposition. In a lower temperature deposition, the viscosity of the ethaline electrolyte was relatively high, with relatively low electrical conductivity. This leads to a slow migration rate and cathodic reaction rate of the metal ions in the electrolyte, resulting in a decreased growth rate of the deposited particles. On the other hand, a higher deposition temperature leads to an increased rate of metal ion migration.

As revealed from the XRD patterns in Figure 2, the annealing process resulted in the complete crystallization of the amorphous titania to anatase, which can increase the stability of the nanotube layer as a result of crystallization. After zinc electrodeposition, pure metallic crystalline zinc was observed, as demonstrated in the zinc peaks in Figure 2.

4.2. CV of Zn/TiO_2 NTAs

In the inset of Figure 4, the CV of TiO_2 NTAs in 0.1 M NaOH presents a reduction peak below 0.03 V. An oxidation peak can be observed above 0.25 V. These two potentials form a redox pair for the bare TiO_2 NTAs. After the addition of 5 mM of glucose, the CV of TiO_2 NTAs presents two reduction peaks below 0.03 V that are most likely described by the hydrogen insertion process. In the anodic sweeping direction, two oxidation peaks can be observed above 0.017 V. The first oxidation peak likely ascribes to the adsorption of hydrogen and glucose on the surface of the TiO_2 NTAs, which has a non-negligible electrocatalytic activity. The second oxidation peak corresponds to the hydrogen disinsertion process [34].

In the case of Zn/TiO_2 NTAs, without the presence of glucose, the redox pair related to TiO_2 NTAs seen in the inset is present between 0.36 V and 0.02 V. An additional oxidation peak in this CV appeared at around 0.68 V, which could be attributed to zinc oxidation [35]. With the addition of 5 mM of glucose, an oxidation peak appeared at around 0.24 V, which could be ascribed to the oxidation of glucose. The drastic increase in the current peak response of Zn/TiO_2 NTAs compared to bare TiO_2 NTAs indicates that zinc NHexs improve the electrocatalytic performance of the TiO_2 NTAs in a glucose-containing environment. This is possibly due to the increase in the Zn^{2+} concentration in the cell, leading to an increased current density near the Zn/TiO_2 NTA electrode surface.

The process of glucose oxidation on Zn/TiO_2 NTAs could be explained by the model proposed by Burke et al. called the "incipient hydrous oxide adatom mediator" (IHOAM) model, which discussed the role of hydroxyl radicals in electrocatalysis [7,36]. The IHOAM process is based on the observation that metal surface atoms undergo a pre-monolayer oxidation step, which results in the formation of an incipient hydrous oxide layer composed of OH_{ads} that mediate glucose electrooxidation and inhibit many kinetically slow reduction processes. At the electrode surface, "active" atoms have a low coordination value and lack lattice stabilization energy. IHOAM predicts that glucose is electrocatalytically oxidized by forming hydrous species on electrode surfaces, followed by glucose chemisorption. The hydrous pre-monolayer then mediates the electrooxidation of absorbed glucose at a significantly low potential, with the metal surface regenerating. During the repetitive cycling process, oxygen species oxidize the metal's surface again at a certain potential while glucose is continuously oxidized.

$$O_{2g} \leftrightarrow O_{2ads}[Zn/(Zn(OH)_2)] \quad (1)$$

$$O_{2ads}[Zn/(Zn(OH)_2)] + 2e^-[Zn/(Zn(OH)_2)] \rightarrow 2O^-_{ads}\left(O^-/O^-_2\right) \quad (2)$$

$$\text{Glucose} + O^- \rightarrow \text{Gluconolactone} + 2e^- \quad (3)$$

$$\text{Gluconolactone} \overset{\text{Hydrolysis}}{\rightarrow} \text{Gluconicacid} \quad (4)$$

In the case of Zn/TiO_2 NTAs, an intermediate layer can form due to the adsorption of OH^- onto the electrode surface, forming $Zn(OH)_2$ with adsorbed oxygen (Equations (1) and (2)), which participates in glucose oxidation to create gluconolactone and give off electron (Equation (3)) [37,38]. The bulk oxygen evolution on the Zn/TiO_2 NTA surface starts contributing to glucose oxidation after it becomes more thermodynamically favorable, compared to the glucose oxidation facilitated by the intermediate layer [39]. The resulting gluconolactone then undergoes spontaneous hydrolysis into gluconic acid (Equation (4)).

A linear relationship between oxidation current peak values (Figure 3) and the square root of scan rates indicates that the oxidation reaction at the electrode surface follows the Randles–Sevcik model, indicative of the diffusion-controlled reaction on the electrode surface. This relationship is also observed in other non-enzymatic glucose sensing materials [31,37,40,41]. From the inset of Figure 5, the limit of detection (LOD) for glucose on the Zn/TiO_2 NTAs can be obtained by:

$$\text{LOD} = 3S_y/N \tag{5}$$

where S_y is the standard deviation of y-intercept and N is the slope of the calibration curve. The limit of detection for glucose (LOD) is calculated to be 0.44 mM, which is low compared to prior multicomponent glucose sensing materials [42,43].

4.3. EIS of Zn/TiO_2 NTAs

As shown in Figure 6, at 1 kHz, the as-anodized TiO_2 NTAs exhibit overall higher normalized impedance compared to the annealed TiO_2 NTAs. This indicates that the annealing process effectively decreased the impedance of the TiO_2 NTAs. At higher frequencies (>100 Hz), the impedance values approached minimum values due to charge transfer activities. The data points at around the 60 Hz frequency were intentionally blocked out during the data collection process in order to minimize the influence from connection wires.

The phase plots in Figure 7 revealed the charge transfer activities of the NTA samples. The phase plots present their peaks at higher frequencies, indicating that the sample was acting as a capacitor at higher frequency ranges. The phase plots of the as-anodized and annealed samples from Figure 7 show that after the annealing process, the samples produced more reproducible and stable phase responses in the frequency range from 10 kHz to 1 kHz. The phase angles of the as-anodized Zn/TiO_2 NTAs at 1 kHz vary noticeably, indicating non-uniformity in the zinc deposits in the as-anodized samples. The room temperature-deposited as-anodized Zn/TiO_2 NTAs also present multiple phase peaks that possibly relate to multiple charge transfers, indicating the existence of an intermediate layer which inhibits singular charge transfer [44]. The presence of zinc NHexs on annealed samples appears to shift both the capacitive and resistive responses of the samples to a lower frequency range. The zinc NHexs deposited at an increased temperature do not appear to have a significant effect on the electrochemical behavior of the resulting Zn/TiO_2 NTA samples.

4.4. Glucose Sensing Performance of Zn/TiO_2 NTAs

Table 1 summarizes the glucose sensing performances of prior multi-component non-enzymatic electrocatalytic material systems as well as that of Zn/TiO_2 NTAs. Compared to some other designs utilizing metal oxides such as CuO (i.e., 234–3218.5 μA mM^{-1} cm^{-2}), the glucose sensitivity of Zn/TiO_2 NTAs in this work is relatively low [24,25,43,45,46]. However, compared to prior implantable non-enzymatic catalyst materials involving zinc oxide nanostructures such as ZnO@C/GCE [47], the sensitivity of the Zn/TiO_2 NTAs in this work (4.38 μA mM^{-1} cm^{-2}) is within the same range or higher. While a linear range of 0.5–5 mM of glucose concentration for Zn/TiO_2 NTAs is not the widest among past non-enzymatic designs involving ZnO [47,48], it is within the glucose range in human blood (4–6 mM) [47]. Moreover, the detection limit (0.44 mM) of Zn/TiO_2 NTAs is lower

compared to prior ZnO and CuO designs, allowing the Zn/TiO_2 NTAs to detect glucose in low concentrations [43,47].

The difference in glucose sensitivity between Cu-based materials and our design could have been the result of different metal/metal oxide concentrations, substrate conductivity, and material architecture. On the other hand, while glucose sensing materials utilizing Cu or CuO show good sensitivity towards glucose with a comparable linear range compared to the Zn/TiO_2 NTAs fabricated in this work, metal Cu and CuO are not suitable for prolonged in vivo glucose sensing operations due to its toxicity in the human body.

Table 1. Comparison of glucose sensing performance of the device in this work with other non-enzymatic glucose sensing designs.

Material Name	Linear Range (mM)	Detection Limit (mM)	Sensitivity ($\mu A\ mM^{-1}\ cm^{-2}$)	Potential (V)	Medium	Ref.
Zn/TiO_2 NTAs	0.5–5	0.44	4.38	0.7	0.1 M NaOH/Glucose	This Work
CuO/Cu/TNT	0.2–90.4	0.019	234	0.42	Acetonitrile/ 0.1 M TEAP	[45]
ZnO/GCE	0.02–4.5	0.02	15.33	0.8	1X PBS/Glucose	[28]
ZnO@C/GCE	0.1–10	1	2.97	0.38	0.1 M NaOH/Glucose	[47]
ZnO nanowire/EμPAD	0–15	5.95×10^{-2}	8.24	0.8	1X PBS/Glucose	[48]
CuO/GCE	0.006–2.5	0.8	431.3	0.4	0.1 M NaOH/Glucose	[43]
Ni/Cu/MWCNT	2.5×10^{-5}–0.8	0.025×10^{-3}	2633	0.575	0.1 M NaOH/Glucose	[46]
Au/CuO	10^{-3}–30	3×10^{-4}	708.7	0.35	1.0 M NaOH/Glucose	[24]
CuO/Cu	0–0.8	5×10^{-4}	3218.5	0.55	1.0 M NaOH/Glucose	[25]
Cu_2O/TiO_2	5–35	8.85×10^{-5}	101.65	0.7	0.1 M NaOH/Glucose	[26]
PVP/TiO_2	0–13	0.76	360.13	0.63	0.1 M NaOH/Glucose	[42]

5. Conclusions

Zinc NHexs have been decorated onto TiO_2 NTAs via an electrodeposition process. A zinc-containing deep eutectic solvent was used to generate the zinc NHexs. CV analysis of Zn/TiO_2 NTAs in 0.1 M NaOH with glucose reveals the possible adsorption of reactant species occurring at the sample surface, fitting the IHOAM model of glucose oxidation. Zn/TiO_2 NTAs were found to be an effective multi-component material system for the glucose oxidation process. When compared to past implantable non-enzymatic glucose oxidizing material designs involving zinc oxide, the electrode produced in this work shows an improvement in the glucose sensitivity (4.38 $\mu A\ mM^{-1}\ cm^{-2}$) within comparable linear ranges (0.5 mM–5 mM) of glucose concentrations to human blood. The detection limit (0.44 mM) of the electrode from this work is lower than some of the metal/metal oxide compounds reported in the literature, indicating an improved ability to detect glucose at lower concentrations. Although the glucose sensitivities of Cu/CuO-based materials are significantly higher than that of the one from this work, metal copper and copper oxide are not biocompatible materials, and as such, are not ideal choices for prolonged operation in implanted devices due to their toxicity in vivo.

Author Contributions: Conceptualization, H.A.H. and K.W.; methodology, H.A.H. and K.W.; validation, H.A.H. and K.W.; formal analysis, H.A.H. and K.W.; investigation, H.A.H. and K.W.; resources, H.A.H.; data curation, H.A.H. and K.W.; writing—original draft preparation, K.W.; writing—review and editing, H.A.H. and K.W.; visualization, H.A.H. and K.W.; supervision, H.A.H.; project administration, H.A.H.; funding acquisition, H.A.H. All authors have read and agreed to the published version of the manuscript.

Funding: This research received no external funding.

Data Availability Statement: Data is contained within the article.

Acknowledgments: The authors would like to acknowledge the support of the staff and use of instruments in the Case Western Reserve University, Case School of Engineering, Swagelok Center for Surface Analysis of Materials (SCSAM) for the collection and analysis of SEM data. The authors would also like to gratefully acknowledge Kenneth Loparo and the Institute for Smart, Secure, and Connected Systems (ISSACS) for providing partial funding support for this project.

Conflicts of Interest: The authors declare no conflicts of interest.

References

1. Heller, A.; Feldman, B. Electrochemical Glucose Sensors and Their Applications in Diabetes Management. *Chem. Rev.* **2008**, *108*, 2482–2505. [CrossRef] [PubMed]
2. Yoo, E.-H.; Lee, S.-Y. Glucose Biosensors: An Overview of Use in Clinical Practice. *Sensors* **2010**, *10*, 4558–4576. [CrossRef] [PubMed]
3. Lee, H.; Hong, Y.J.; Baik, S.; Hyeon, T.; Kim, D.-H. Enzyme-Based Glucose Sensor: From Invasive to Wearable Device. *Adv. Healthc. Mater.* **2018**, *7*, 1701150. [CrossRef]
4. Hassan, M.H.; Vyas, C.; Grieve, B.; Bartolo, P. Recent Advances in Enzymatic and Non-Enzymatic Electrochemical Glucose Sensing. *Sensors* **2021**, *21*, 4672. [CrossRef] [PubMed]
5. Riddell, M.C.; Scott, S.N.; Fournier, P.A.; Colberg, S.R.; Gallen, I.W.; Moser, O.; Stettler, C.; Yardley, J.E.; Zaharieva, D.P.; Adolfsson, P.; et al. The competitive athlete with type 1 diabetes. *Diabetologia* **2020**, *63*, 1475–1490. [CrossRef]
6. Nichols, S.P.; Koh, A.; Storm, W.L.; Shin, J.H.; Schoenfisch, M.H. Biocompatible Materials for Continuous Glucose Monitoring Devices. *Chem. Rev.* **2013**, *113*, 2528–2549. [CrossRef]
7. Si, P.; Huang, Y.; Wang, T.; Ma, J. Nanomaterials for electrochemical non-enzymatic glucose biosensors. *RSC Adv.* **2013**, *3*, 3487–3502. [CrossRef]
8. Wang, G.; He, X.; Wang, L.; Gu, A.; Huang, Y.; Fang, B.; Geng, B.; Zhang, X. Non-enzymatic electrochemical sensing of glucose. *Microchim. Acta* **2013**, *180*, 161–186. [CrossRef]
9. Park, S.; Boo, H.; Chung, T.D. Electrochemical non-enzymatic glucose sensors. *Anal. Chim. Acta* **2006**, *556*, 46–57. [CrossRef]
10. Govindaraj, M.; Srivastava, A.; Muthukumaran, M.K.; Tsai, P.-C.; Lin, Y.-C.; Raja, B.K.; Rajendran, J.; Ponnusamy, V.K.; Selvi, J.A. Current advancements and prospects of enzymatic and non-enzymatic electrochemical glucose sensors. *Int. J. Biol. Macromol.* **2023**, *253*, 126680. [CrossRef]
11. Gloeb-McDonald, R.G.; Fridman, G. Glucose Fuel Cells: Electricity from Blood Sugar. *IEEE Rev. Biomed. Eng.* **2024**. *online ahead of prints*. [CrossRef] [PubMed]
12. Dong, Q.; Ryu, H.; Lei, Y. Metal oxide based non-enzymatic electrochemical sensors for glucose detection. *Electrochim. Acta* **2021**, *370*, 137744. [CrossRef]
13. Jiang, J.; Li, Y.; Liu, J.; Huang, X.; Yuan, C.; Lou, X.W. Recent Advances in Metal Oxide-based Electrode Architecture Design for Electrochemical Energy Storage. *Adv. Mater.* **2012**, *24*, 5166–5180. [CrossRef] [PubMed]
14. Zhang, G.; Xiao, X.; Li, B.; Gu, P.; Xuea, H.; Pang, H. Transition metal oxides with one-dimensional/one-dimensional-analogue nanostructures for advanced supercapacitors. *J. Mater. Chem. A Mater.* **2017**, *5*, 8155–8186. [CrossRef]
15. Kant, K.; Priest, C.; Shapter, J.; Losic, D. The Influence of Nanopore Dimensions on the Electrochemical Properties of Nanopore Arrays Studied by Impedance Spectroscopy. *Sensors* **2014**, *14*, 21316–21328. [CrossRef]
16. Fazio, E.; Spadaro, S.; Corsaro, C.; Neri, G.; Leonardi, S.G.; Neri, F.; Lavanya, N.; Sekar, C.; Donato, N.; Neri, G. Metal-Oxide Based Nanomaterials: Synthesis, Characterization and Their Applications in Electrical and Electrochemical Sensors. *Sensors* **2021**, *21*, 2494. [CrossRef]
17. Yuan, F.; Xia, Y.; Lu, Q.; Xu, Q.; Shu, Y.; Hu, X. Recent advances in inorganic functional nanomaterials based flexible electrochemical sensors. *Talanta* **2022**, *244*, 123419. [CrossRef]
18. He, C.; Asif, M.; Liu, Q.; Xiao, F.; Liu, H.; Xia, B.Y. Noble Metal Construction for Electrochemical Nonenzymatic Glucose Detection. *Adv. Mater. Technol.* **2023**, *8*, 2200272. [CrossRef]
19. Wang, Y.; Chen, J.; Zhou, C.; Zhou, L.; Kong, Y.; Long, H.; Zhong, S. A novel self-cleaning, non-enzymatic glucose sensor working under a very low applied potential based on a Pt nanoparticle-decorated TiO_2 nanotube array electrode. *Electrochim. Acta* **2014**, *115*, 269–276. [CrossRef]
20. Grochowska, K.; Ryl, J.; Karczewski, J.; Śliwiński, G.; Cenian, A.; Siuzdak, K. Non-enzymatic flexible glucose sensing platform based on nanostructured TiO_2–Au composite. *J. Electroanal. Chem.* **2019**, *837*, 230–239. [CrossRef]
21. Bertel, L.; Miranda, D.A.; García-Martín, J.M. Nanostructured Titanium Dioxide Surfaces for Electrochemical Biosensing. *Sensors* **2021**, *21*, 6167. [CrossRef] [PubMed]

22. Cheng, Y.; Yang, H.; Yang, Y.; Huang, J.; Wu, K.; Chen, Z.; Wang, X.; Lin, C.; Lai, Y. Progress in TiO_2 nanotube coatings for biomedical applications: A review. *J. Mater. Chem. B* **2018**, *6*, 1862–1886. [CrossRef] [PubMed]
23. Ndolomingo, M.J.; Bingwa, N.; Meijboom, R. Review of supported metal nanoparticles: Synthesis methodologies, advantages and application as catalysts. *J. Mater. Sci.* **2020**, *55*, 6195–6241. [CrossRef]
24. Li, Z.; Xin, Y.; Zhang, Z.; Wu, H.; Wang, P. Rational design of binder-free noble metal/metal oxide arrays with nanocauliflower structure for wide linear range nonenzymatic glucose detection. *Sci. Rep.* **2015**, *5*, 10617. [CrossRef] [PubMed]
25. Wang, J.; Zhang, W.-D. Fabrication of CuO nanoplatelets for highly sensitive enzyme-free determination of glucose. *Electrochim. Acta* **2011**, *56*, 7510–7516. [CrossRef]
26. Kumar, B.; Sinha, S.K. Nanostructured Cu_2O deposited on TiO_2 nanotube arrays for ultra-sensitive non-enzymatic glucose electrochemical biosensor. *Ionics* **2022**, *29*, 793–805. [CrossRef]
27. Song, L.; Connolly, M.; Fernández-Cruz, M.L.; Vijver, M.G.; Fernández, M.; Conde, E.; de Snoo, G.R.; Peijnenburg, W.J.; Navas, J.M. Species-specific toxicity of copper nanoparticles among mammalian and piscine cell lines. *Nanotoxicology* **2014**, *8*, 383–393. [CrossRef]
28. Wang, J.X.; Sun, X.W.; Wei, A.; Lei, Y.; Cai, X.P.; Li, C.M.; Dong, Z.L. Zinc oxide nanocomb biosensor for glucose detection. *Appl. Phys. Lett.* **2006**, *88*, 233106. [CrossRef]
29. Dang, T.K.; Van Toan, N.; Hung, C.M.; Van Duy, N.; Viet, N.N.; Thong, L.V.; Son, N.T.; Van Hieu, N.; Le Manh, T. Investigation of zinc electronucleation and growth mechanisms onto platinum electrode from a deep eutectic solvent for gas sensing applications. *J. Appl. Electrochem.* **2022**, *52*, 299–309. [CrossRef]
30. Wang, K.; Phelps, J.; Abdolvand, R.; Carter, J.; Amani Hamedani, H. Zinc Nanoparticles Electrodeposited on TiO_2 Nanotube Arrays Using Deep Eutectic Solvents for Implantable Electrochemical Sensors. *ACS Appl. Nano Mater.* **2023**, *6*, 8238–8249. [CrossRef]
31. Lavanya, N.; Leonardi, S.; Marini, S.; Espro, C.; Kanagaraj, M.; Reddy, S.L.; Sekar, C.; Neri, G. $MgNi_2O_3$ nanoparticles as novel and versatile sensing material for non-enzymatic electrochemical sensing of glucose and conductometric determination of acetone. *J. Alloys Compd.* **2020**, *817*, 152787. [CrossRef]
32. Long, M.; Tan, L.; Liu, H.; He, Z.; Tang, A. Novel helical TiO_2 nanotube arrays modified by Cu_2O for enzyme-free glucose oxidation. *Biosens. Bioelectron.* **2014**, *59*, 243–250. [CrossRef] [PubMed]
33. Pradhan, R.; Mitra, A.; Das, S. Impedimetric characterization of human blood using three-electrode based ECIS devices. *J. Electr. Bioimped.* **2012**, *3*, 12–19. [CrossRef]
34. Hanzu, I.; Djenizian, T.; Knauth, P. Electrical and Point Defect Properties of TiO_2 Nanotubes Fabricated by Electrochemical Anodization. *J. Phys. Chem. C* **2011**, *115*, 5989–5996. [CrossRef]
35. Doche, M.-L.; Hihn, J.-Y.; Touyeras, F.; Lorimer, J.; Mason, T.; Plattes, M. Electrochemical behaviour of zinc in 20 kHz sonicated NaOH electrolytes. *Ultrason. Sonochem.* **2001**, *8*, 291–298. [CrossRef]
36. Burke, L.D. Premonolayer oxidation and its role in electrocatalysis. *Electrochim. Acta* **1994**, *39*, 1841–1848. [CrossRef]
37. Liang, Z.; Zhang, X. Zn–ZnO@TiO_2 nanocomposite: A direct electrode for nonenzymatic biosensors. *J. Mater. Sci.* **2018**, *53*, 7138–7149. [CrossRef]
38. Song, Y.-Y.; Zhang, D.; Gao, W.; Xia, X.-H. Nonenzymatic Glucose Detection by Using a Three-Dimensionally Ordered, Macroporous Platinum Template. *Chem.-Eur. J.* **2005**, *11*, 2177–2182. [CrossRef]
39. Bard, A.J.; Faulkner, L.R.; White, H.S. *Electrochemical Methods: Fundamentals and Applications*; John Wiley & Sons: Hoboken, NJ, USA, 2022.
40. Li, X.; Yao, J.; Liu, F.; He, H.; Zhou, M.; Mao, N.; Xiao, P.; Zhang, Y. Nickel/Copper nanoparticles modified TiO_2 nanotubes for non-enzymatic glucose biosensors. *Sens. Actuators B Chem.* **2013**, *181*, 501–508. [CrossRef]
41. Arthanari, S.; Sivaprakasam, R.; Park, J.; Yang, M.; Lee, H.; Kim, B.; Hwang, J.S. Fabrication of Porous Non-Enzymatic Glucose Sensing Electrodes Through Nanosecond-Laser Patterning of Metal–Organic Frameworks. *Adv. Mater. Technol.* **2024**, *9*, 98563–98580. [CrossRef]
42. Yadav, M.; Singh, G.; Lata, S. Polyvinylpyrrolidone/TiO_2 composites' preparation via sol–gel procedure furthered with non-enzymatic glucose sensing and antibacterial effectiveness. *Environ. Sci. Pollut. Res.* **2022**, *25*, 708–714. [CrossRef] [PubMed]
43. Wang, W.; Zhang, L.; Tong, S.; Li, X.; Song, W. Three-dimensional network films of electrospun copper oxide nanofibers for glucose determination. *Biosens. Bioelectron.* **2009**, *25*, 708–714. [CrossRef]
44. Li, F.-H.; Wang, W.; Gao, J.-P.; Wang, S.-Y. Electrochemical Reduction Process of Sb(III) on Au Electrode Investigated by CV and EIS. *J. Electrochem. Soc.* **2009**, *156*, D84. [CrossRef]
45. Zhou, Z.; Zhu, Z.; Cui, F.; Shao, J.; Zhou, H.S. CuO/Cu composite nanospheres on a TiO_2 nanotube array for amperometric sensing of glucose. *Microchim. Acta* **2020**, *187*, 123. [CrossRef] [PubMed]
46. Lin, K.-C.; Lin, Y.-C.; Chen, S.-M. A highly sensitive nonenzymatic glucose sensor based on multi-walled carbon nanotubes decorated with nickel and copper nanoparticles. *Electrochim. Acta* **2013**, *96*, 164–172. [CrossRef]

47. Chung, R.-J.; Wang, A.-N.; Liao, Q.-L.; Chuang, K.-Y. Non-Enzymatic Glucose Sensor Composed of Carbon-Coated Nano-Zinc Oxide. *Nanomaterials* **2017**, *7*, 36. [CrossRef]
48. Li, X.; Zhao, C.; Liu, X. A paper-based microfluidic biosensor integrating zinc oxide nanowires for electrochemical glucose detection. *Microsyst. Nanoeng.* **2015**, *1*, 15014. [CrossRef]